Short-Term PV Power Forecasts Based on a Real-Time Irradiance Monitoring Network

Antonio T. Lorenzo*, William F. Holmgren†, Michael Leuthold‡,
Chang Ki Kim‡, Alexander D. Cronin†, Eric A. Betterton‡

*College of Optical Sciences, University of Arizona, Tucson, AZ, United States
†Department of Physics, University of Arizona, Tucson, AZ, United States
‡Department of Atmospheric Sciences, University of Arizona, Tucson, AZ, United States

***Abstract*—We built an irradiance sensor network that we are now using to make operational, real-time, intra-hour forecasts of solar power at key locations. We developed reliable irradiance sensor hardware platforms to enable these sensor network forecasts. Using 19 of the 55 irradiance sensors we have throughout Tucson, we make retrospective forecasts of 26 days in April and evaluate their performance. We find that that our network forecasts outperform a persistence model for 1 to 28 minute time horizons as measured by the root mean squared error. The sensor hardware, our network forecasting method, error statistics, and future improvements to our forecasts are discussed.**

***Index Terms*—data analysis, forecasting, real-time systems, sensors, solar energy.**

I. Introduction

The demand for high accuracy solar power forecasting services is increasing as electric utilities and independent service operators add more variable and potentially destabilizing solar power generation. Numerous forecasting methods are being actively developed including those based on artificial neural networks [1], total sky imagers [2]–[5], irradiance sensor networks [6], [7], satellite derived irradiance [8], numerical weather models [9], and hybrid methods [10]. Each method has an optimal forecasting horizon; often, total sky imagers and irradiance sensor network forecasts perform best for very short (5-30 minutes) time horizons, satellite forecasts perform best for short- to mid-term horizons (1-4 hours), and numerical weather models perform best for longer horizons (>4 hours). The optimal horizon for neural networks and hybrid methods varies.

In our preliminary study [6], we made retrospective forecasts using 15 minute data from rooftop PV systems that performed optimally for 45 minute time horizons. In this paper, we describe our *operational* forecasts that are made using an improved sensor network that reports in real-time. We evaluate forecasts from 26 days in April that were made retrospectively. Preliminary evaluation presented here shows that our network forecasts outperform a persistence forecast for 1 to 28 minute time horizons. We attribute this difference in performance compared to our earlier study to the smaller network used in the study. Our previous study was also restricted to 15 minute averaged data that hides some solar variability.

In Section II, we describe our irradiance monitoring network and the sensors we developed. Then, we explain our method to generate irradiance network forecasts in Section III. Error statistics are presented in Section IV, and conclusions and future work are discussed in Section V.

II. Irradiance Monitoring Network

A major barrier to making irradiance network based PV power forecasts is obtaining irradiance data in near real-time with high spatial and temporal resolution. We currently have a network of 55 sensors throughout the Tucson region that we use to make operational network forecasts. In this concentrated study, we use a subset of 19 sensors near the University of Arizona Science and Technology Park (UASTP). Our sensors are made up of irradiance network nodes (INNs) that we developed, rooftop PV system power data direct from monitoring equipment, and utility-scale PV power data. We now describe the INN hardware we developed to make network forecasts, the central database where all irradiance data is stored, and the network used in this study.

A. Sensor Hardware

To make high-quality network forecasts, we need reliable sensor hardware that reports in nearly real-time. We chose to design our own hardware after researching existing solutions in the market and finding them unsuitable or too expensive. Our sensor hardware is relatively cheap, uses reliable Linux microcomputers, and requires minimal maintenance. It is also worth noting that our current sensors are not meant to be accurate global irradiance sensors, although with careful mounting and a suitable pyranometer, they can be. A summary of the sensor hardware is presented in Table I.

TABLE I
Summary of Irradiance Network Nodes

Model	Comms. Backend	Sensor Type	Processing Unit	Collection Period
Saguaro	Cellular data network	Pyranometer or photodiode	iMX233-OLinuXino-MICRO	1 second
Prickly Pear	Ethernet internet connection	Rooftop PV power measurement	Raspberry Pi	10 seconds
Yucca	Ethernet internet connection	Pyranometer or photodiode	Raspberry Pi	1 second

The Saguaro INN is designed to be placed in remote locations and communicate via cellular data networks. We use either a calibrated pyranometer (Apogee SP-212) or a cheap silicon photodiode (Osram BPW34) to monitor the irradiance at the location of the sensor. We use an appropriate trans-impedance amplifier to convert the current from the photodiode to a measurable voltage. Voltage data from the sensor is read every second from a program running on an Olimex iMX233-OLinuXino-MICRO via an analog to digital converter. This data is sent every minute via a cellular modem (Multi-Tech MTSMC-H5) to our central database. This hardware is co-located on a custom PCB along with a DC-DC switching power supply, a board temperature monitor, and a battery voltage monitor. A 10W solar panel, 6Ah, 12V lead acid battery, and solar charge controller provide power to the hardware that consumes less than 1W of power on average. A picture of the Saguaro INN is shown in Fig. 1.

Fig. 1. Picture of the Saguaro INN. The solar panel that provides power to the unit and the sensor attached to the stalk are visible.

The Prickly Pear and Yucca INNs both send data over the internet using a Raspberry Pi, but use different sensors. The Prickly Pear INN communicates over Ethernet to a rooftop PV system's monitoring hardware (e.g. SMA Sunny WebBox) to use PV power as a proxy for irradiance. The Yucca INN uses a pyranometer or photodiode, like the Saguaro INN, that is read via an Arduino FIO placed in the sun and transfered via XBee to the central unit. The Prickly Pear and Yucca both use a cheap Linux computer (Raspberry Pi) as the central collection point.

All three INNs use the Arch Linux operating system with custom kernels. Most programs are written in Python. We currently use SFTP to transfer the data from the sensor to our central database every minute. In the future we will use the messaging service ZeroMQ to transfer data with lower latency. We can update the software remotely using Fabric, and we use SSH to remotely log-in to a sensor if needed. We also have scripts on the Saguaro INN that monitor the cellular data connection, the board temperature, and the battery voltage. The INNs only send data during the day (as calculated by ephemeris code for each day) to save power and network bandwidth.

B. Central Database

As soon as data is sent to our central server via SFTP or ZeroMQ, a script loads the one-second data into a MySQL database. The data is identified by a sensor ID number, epoch time stamp, and measurement. We also keep a MySQL table to store metadata for each sensor including location, sensor type, etc., and a table to store battery charge levels and temperatures for Saguaro INNs.

C. Network Used in this Study

A map of the 19 sensors used in this focused study is shown in Fig. 2. Most of the sensors are Saguaro INNs, although some are 5-minute data from rooftop PV systems, and 2-second power data from utility-scale installations. Forecasts were analyzed for locations at the UASTP, shown in Fig. 2b. We use a higher density of sensors to the southwest of the UASTP because the primary wind direction is from the southwest.

III. Sensor Network Forecasts

Here we describe how we generate our network forecasts, which is similar to our previous method described in [6]. First, we generate clear-sky expectations for each sensor using data from clear days. Operationally, these are generated roughly weekly and checked visually. This data driven approach captures shading due to obstacles, orientation, and other system specific parameters. At each specified time step t (every 1 minute in this study), we calculate the clearness index for each sensor n as

$$K_n(t) = \frac{g_n(t)}{g_{n,clear}(t)} \tag{1}$$

where $g_n(t)$ is the measured data at time t and $g_{n,clear}(t)$ is the clear-sky expectation at time t. In this study, the measured data is the average of the data collected over the previous one minute. Once the clearness is calculated for each sensor, we use bivariate interpolation to make an interpolated clearness map similar to Fig. 3. We set the boundary of this map using the average clearness of all sensors for the previous minute. We can also use satellite images or numerical weather models to set this boundary. Then, we forecast the clearness for a sensor or arbitrary location by propagating this clearness map using an assumed cloud motion vector. There are a number of ways we could calculate this cloud motion vector, and we describe some methods we will explore in future work in

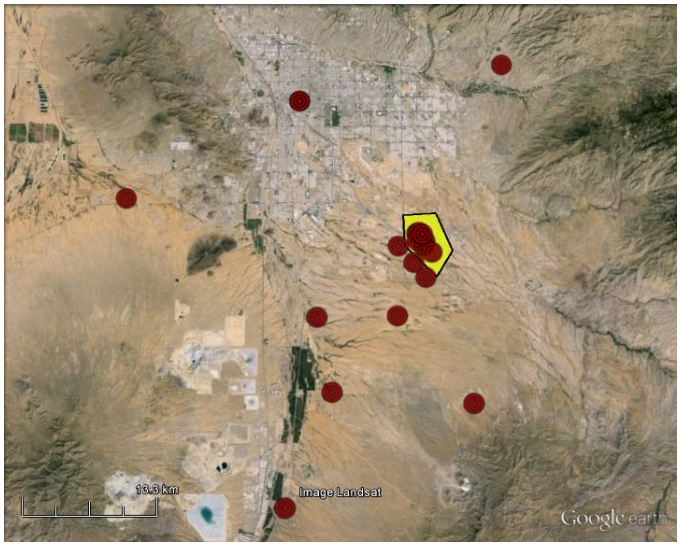

(a) Full Sensor Map

(b) Detailed UASTP Map

Fig. 2. Map of sensors used in this study throughout the Tucson area. A more detailed map of the UA Science and Technology Park (UASTP) highlighted in (a) is shown in (b).

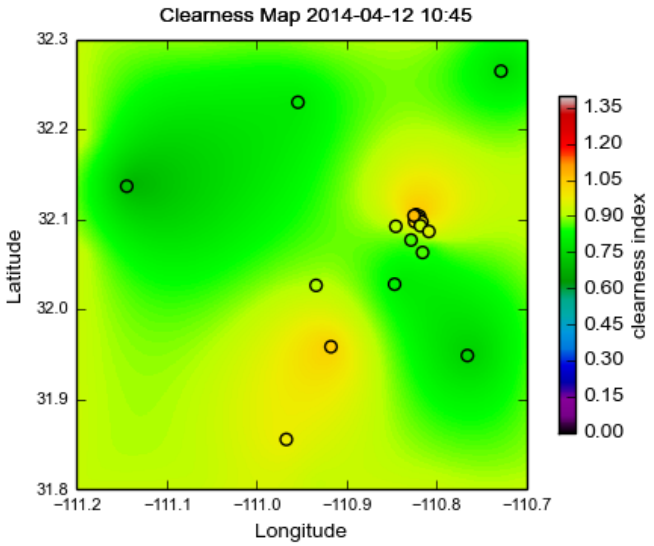

Fig. 3. Example interpolated clearness map.

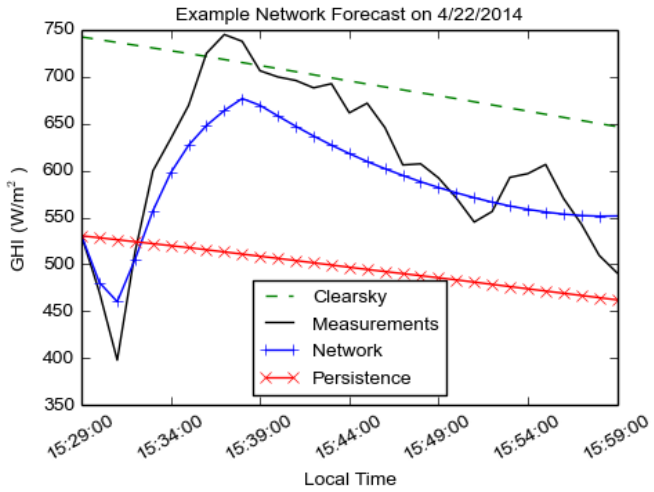

Fig. 4. Example forecasts made for a 30 minute period on 4/22/2014. The network forecast, clearness persistence forecast, clear-sky expectation, and measured data are shown. Forecasts shown are made at 15:29.

Section V. Here, we use the hourly output of a custom, high-resolution Weather Research and Forecasting (WRF) model that are produced earlier in the day to determine this cloud motion vector. To make this determination, we find the most likely cloud base height and then use the wind speed and direction at this height as the cloud motion vector. Finally, we calculate the quantity of interest (power or irradiance) with this forecasted clearness and the clear-sky expectation. We repeat this procedure for each forecast horizon. For this study, this means that we calculate the a new forecast every minute during the day for each of the next thirty minutes. A single example forecast for a Saguaro INN for a cloudy day in April is plotted in Fig. 4. A full day of 10-minute ahead forecasts is shown in Fig. 5.

IV. Error Statistics

We now present error statistics for GHI forecasts made for 26 days in April. Of these days, 10 days had completely clear skies, 8 days were variable due to high, thin cirrus clouds, 2 days were overcast, and the remaining 6 days were highly variable. Data used to calculate and evaluate the forecasts were binned into 1 minute averages. Forecasts were calculated and evaluated for each minute of the day for forecast horizons from 0 to 30 minutes. Forecast error metrics were calculated for each day and then averaged for the month. Only daylight hours were considered. In addition to evaluating our network forecasts, we also evaluate a clear-sky model and two persistences models: a clearness based model that assumes the clearness is constant and a measurement based model that

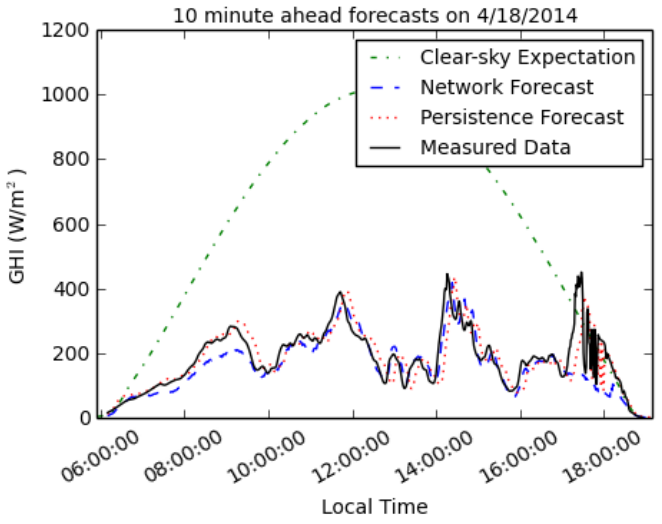

Fig. 5. Example 10 minute ahead forecasts made on 4/18/2014. The network forecast, clearness persistence forecast, clear-sky expectation, and measured data are shown. The forecasts for 10 minutes in the future are made every minute.

assumes the measured irradiance is constant. Obviously, the measurement persistence model will have larger errors and less skill than a clearness persistence model as forecast horizon increases because it does not account for the diurnal cycle. For comparison, the clear-sky forecast model simply assumes that any future irradiance will be the same as the clear-sky expectation. We also compared our network forecasts to the first day of 3 minute irradiance forecast produce by our WRF model.

The mean absolute error (MAE) and root mean squared error (RMSE) (using the standard definitions as found in [11]) for forecast horizons that are multiples of 5 are shown in Table II for a single sensor. A plot of MAE vs forecast time horizon is shown in Fig. 6 and a plot of RMSE vs forecast time horizon is shown in Fig. 7. The clearness persistence MAE and RMSE at the 0 minute forecast horizon is not identically zero because we limit the clearness to a maximum of 1.1 and errors in the clear-sky expectation in the early morning and late evening often result in a calculated clearness in excess of this 1.1 limit. Since we then use this 1.1 clearness to calculate the expected irradiance, our expectation and the actual measurement do not match leading to small errors. The network forecast is similarly affected by this clipping, but the larger error at the 0 minute horizon is due to the interpolation we use to make clearness maps. Since this interpolation is smoothed to best fit all sensors, the calculated clearness does not always match the measured clearness. Despite these errors, it is encouraging that our irradiance network based forecasts outperform the persistence model for the days studied for 1 to 28 minutes as measured by RMSE and 2 to 17 minutes as measured by MAE.

TABLE II
ERROR STATISTICS FOR 26 DAYS IN APRIL FOR PERSISTENCE AND NETWORK FORECASTS.

	Clearness Persistence		**Network Forecast**	
Forecast Horizon	MAE (W/m^2)	RMSE (W/m^2)	MAE (W/m^2)	RMSE (W/m^2)
0 min	0.166	1.23	3.26	11.3
5 min	30.4	58.6	**27.6**	**48.1**
10 min	38.7	69.1	**36.6**	**60.0**
15 min	43.6	74.8	**43.0**	**67.9**
20 min	47.7	79.0	50.0	**74.7**
25 min	50.6	81.3	54.1	**78.6**
30 min	52.9	83.2	60.1	85.4

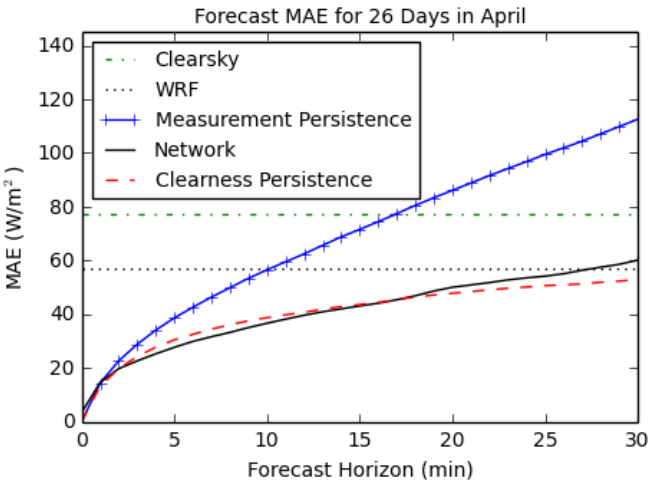

Fig. 6. Mean absolute error as a function of forecast horizon for a single sensor calculated each day and averaged over 26 days in April.

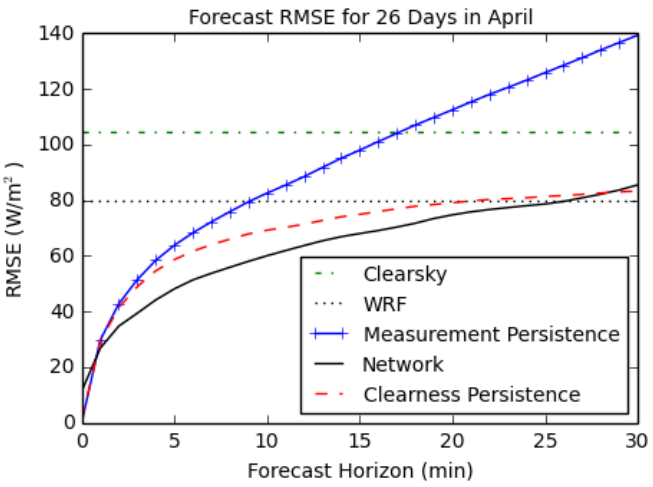

Fig. 7. Root mean squared error as a function of forecast horizon for a single sensor calculated each day and averaged over 26 days in April.

V. Conclusions

We designed and built low-cost irradiance sensors in order to make irradiance network forecasts. Using this network, we have been making operational forecasts since the beginning of 2014. A retrospective analysis for 26 days in April shows that our forecasts often perform better than a persistence model. This work seems to show that our method is better than using a cloud camera as in [4], but one must remember that our error statistics were calculated for irradiance and not clearness. This essentially weights our MAE and RMSE by the time of day. In the near future, we will re-evaluate our forecasts to make a more direct comparision with other work. We will also calculate numerous metrics that are described in [11] and [12] for further comparison with other techniques.

While our results of intra-hour forecasts with a network of irradiance sensors are encouraging, there are still many improvements to be made. We are satisfied with the operation of our custom INNs, but we need to deploy more throughout the Tucson region for higher quality forecasts that perform better at forecast horizons approaching one hour. There are also numerous improvements that we can explore for our forecasting algorithm including:

1) More accurate cloud motion vectors from ground sensor correlations, upper-air soundings, WRF forecasts, artificial neural networks, or some combination
2) Improved clearness map boundaries that incorporate satellite derived irradiance
3) Clearness map interpolation techniques that use previous measurements more wisely to fill in gaps.

These improved operational forecasts will provide a benchmark for network based models.

References

[1] L. Ciabattoni, M. Grisostomi, G. Ippoliti, S. Longhi, and E. Mainardi, "Online tuned neural networks for PV plant production forecasting," in *Photovoltaic Specialists Conference (PVSC), 2012 38th IEEE*. IEEE, 2012, pp. 002 916–002 921. [Online]. Available: http://ieeexplore.ieee.org/xpls/abs_all.jsp?arnumber=6318197

[2] C. W. Chow, B. Urquhart, M. Lave, A. Dominguez, J. Kleissl, J. Shields, and B. Washom, "Intra-hour forecasting with a total sky imager at the UC San Diego solar energy testbed," *Solar Energy*, vol. 85, no. 11, pp. 2881–2893, 2011. [Online]. Available: http://www.sciencedirect.com/science/article/pii/S0038092X11002982

[3] R. Marquez and C. F. Coimbra, "Intra-hour DNI forecasting based on cloud tracking image analysis," *Solar Energy*, vol. 91, pp. 327–336, 2013. [Online]. Available: http://www.sciencedirect.com/science/article/pii/S0038092X1200343X

[4] H. Yang, B. Kurtz, D. Nguyen, B. Urquhart, C. W. Chow, M. Ghonima, and J. Kleissl, "Solar irradiance forecasting using a ground-based sky imager developed at UC San Diego," *Solar Energy*, vol. 103, pp. 502–524, 2014. [Online]. Available: http://www.sciencedirect.com/science/article/pii/S0038092X14001327

[5] S. Quesada-Ruiz, Y. Chu, J. Tovar-Pescador, H. Pedro, and C. Coimbra, "Cloud-tracking methodology for intra-hour DNI forecasting," *Solar Energy*, vol. 102, pp. 267–275, 2014. [Online]. Available: http://www.sciencedirect.com/science/article/pii/S0038092X14000486

[6] V. Lonij, A. E. Brooks, A. D. Cronin, M. Leuthold, and K. Koch, "Intra-hour forecasts of solar power production using measurements from a network of irradiance sensors," *Solar Energy*, vol. 97, pp. 58–66, 2013. [Online]. Available: http://www.sciencedirect.com/science/article/pii/S0038092X13003125

[7] D. Yang, Z. Dong, T. Reindl, P. Jirutitijaroen, and W. M. Walsh, "Solar irradiance forecasting using spatio-temporal empirical kriging and vector autoregressive models with parameter shrinkage," *Solar Energy*, vol. 103, pp. 550–562, 2014. [Online]. Available: http://www.sciencedirect.com/science/article/pii/S0038092X14000425

[8] R. Perez, S. Kivalov, J. Schlemmer, K. Hemker Jr, D. Renné, and T. E. Hoff, "Validation of short and medium term operational solar radiation forecasts in the US," *Solar Energy*, vol. 84, no. 12, pp. 2161–2172, 2010. [Online]. Available: http://www.sciencedirect.com/science/article/pii/S0038092X10002823

[9] P. Mathiesen and J. Kleissl, "Evaluation of numerical weather prediction for intra-day solar forecasting in the continental united states," *Solar Energy*, vol. 85, no. 5, pp. 967–977, 2011. [Online]. Available: http://www.sciencedirect.com/science/article/pii/S0038092X11000570

[10] Y. Chu, H. T. Pedro, and C. F. Coimbra, "Hybrid intra-hour DNI forecasts with sky image processing enhanced by stochastic learning," *Solar Energy*, vol. 98, pp. 592–603, 2013. [Online]. Available: http://www.sciencedirect.com/science/article/pii/S0038092X13004325

[11] J. Zhang, B.-M. Hodge, A. Florita, S. Lu, H. F. Hamann, and V. Banunarayanan, "Metrics for evaluating the accuracy of solar power forecasting," in *3rd International Workshop on Integration of Solar Power into Power Systems*, London, England, October 2013. [Online]. Available: http://www.nrel.gov/docs/fy14osti/60142.pdf

[12] R. Marquez and C. F. Coimbra, "Proposed metric for evaluation of solar forecasting models," *Journal of Solar Energy Engineering*, vol. 135, no. 1, p. 011016, 2013. [Online]. Available: http://solarenergyengineering.asmedigitalcollection.asme.org/article.aspx?articleid=1662255